JOURNAL OF MATERIALS SCIENCE **39** (2004) 5057–5065

The magnetic behaviour of nanostructured zinc ferrite†

M. HOFMANN
Technische Universität München, ZWE, FRM-II, 85747 Garching, Germany

S. J. CAMPBELL*
Technische Universität München, ZWE, FRM-II, 85747 Garching, Germany; School of Physical, Environmental and Mathematical Sciences, University of New South Wales, Australian Defence Force Academy, Canberra ACT 2600, Australia
E-mail: Stewart.Campbell@frm2.tum.de; Stewart.Campbell@adfa.edu.au

H. EHRHARDT
School of Physical, Environmental and Mathematical Sciences, University of New South Wales, Australian Defence Force Academy, Canberra ACT 2600, Australia; Institut für Nanotechnologie, Forschungszentrum Karlsruhe GmbH Postfach 3640, D-76021 Karlsruhe, Germany

R. FEYERHERM
Hahn-Meitner-Institut, BENSC, Glienickerstr. 100, 14109 Berlin, Germany

We have investigated a series of nanostructured $ZnFe_2O_4$ samples produced by mechanical activation (mean particle sizes $d \sim$ 50–8 nm) by variable temperature neutron diffraction measurements (2–535 K) supported by DC magnetisation measurements (4.2–300 K). The systematic increase in the mean inversion parameter ($c \sim 0.04$–0.43) with increasing milling time is accompanied by a gradual decrease in the occurrence of the long range antiferromagnetic ordering observed in the starting $ZnFe_2O_4$ material, as well as a gradual decrease in the related diffuse short range order peak. The neutron diffraction patterns of particles with $d < \sim$15 nm and $c > \sim$0.2 are consistent with the occurrence of ferrimagnetic order and exchange interactions of the type Fe^{3+}(A)–O^{2-}–Fe^{3+} [B]. Diagrams summarising the magnetic regions of nanostructured $ZnFe_2O_4$ are presented. The magnetic behaviour overall agrees well with the enhanced magnetisation and ferromagnetic behaviour reported for nanostructured, ultrafine and thin films of $ZnFe_2O_4$ by other groups using mainly magnetisation and Mössbauer spectroscopy measurements.

1. Introduction

Belying its apparent simplicity as a familiar normal oxide spinel, interest in zinc ferrite, $ZnFe_2O_4$, has continued unabated over the past two decades or so. While $ZnFe_2O_4$ is an important technological material with applications, for example, as a regenerable absorbent material for desulphurisation of hot coal gases [1–3], prime interest in recent years has focussed on delineation of the structural and magnetic properties of $ZnFe_2O_4$, both in its equilibrium and nanostructured or nanocrystalline states. Indeed developments in materials processing and synthesis techniques which result in nanostructured materials, such as those based on ball milling [e.g. 4], have contributed to the continuing interest and investigation of $ZnFe_2O_4$.

As discussed below, mechanical treatments have played an important role in the continuing exploration of $ZnFe_2O_4$. Besides providing insight to changes in chemical [5] and reactive behaviour [1, 6], systematic studies by mechanical processing—either by way of milling polycrystalline $ZnFe_2O_4$or by mechanosynthesis of $ZnFe_2O_4$ (produced by milling mixtures of typically ZnO and α-Fe_2O_3)—have led to new information on the structural and magnetic properties of nanoscale $ZnFe_2O_4$ [e.g. 7–13]. Commensurate with these studies, investigations have been carried out on ultrafine or nanocrystalline $ZnFe_2O_4$ particles prepared by a variety of methods including: the co-precipitation method [14], the critical sol-gel processing or aerogel method [15, 16], a hydrothermal process (see Yu *et al.* [17], who present a summary of the main methods of preparation of spinel ferrites), and a new co-precipitation method using urea [18].

The common feature to the above studies, and one of the main stimuli to the continuing interest, is the enhancement in magnetic properties observed in

†This paper is dedicated to Professor Dr. Philipp Gütlich on the occasion of his 70^{th} birthday.
*Author to whom all correspondence should be addressed.

nanostructured or nanocrystalline particles compared with the magnetic behaviour exhibited by equilibrium $ZnFe_2O_4$. Indeed similar enhancement in magnetisation has also been observed recently in thin films of $ZnFe_2O_4$ prepared by rf sputtering [19]. While many factors contribute to this enhanced magnetisation, the prime factor appears to be linked with the nonequilibrium distribution of the magnetic iron and diamagnetic zinc cations [e.g. 8, 11, 13].

The crystallographic structure of a spinel compound is well known. In familiar notation a spinel can be represented by the formula $(A)[B_2]O_4$ where A and B denote divalent and trivalent cations respectively and the round and the square brackets denote tetrahedral and octahedral sites. The Bravais lattice of the conventional unit cell is a face-centred cubic array of anions with holes partly filled by the cations. Sickafus *et al.* [20] have recently presented a comprehensive review of the crystal structure of a spinel including the interrelationships between the three main degrees of freedom: the lattice parameter, a; the anion parameter, u; and the cation inversion parameter, c. For a normal spinel such as $ZnFe_2O_4$, the A atoms (Zn^{2+}) are tetrahedrally coordinated while the B atoms [Fe^{3+}] are octahedrally surrounded by oxygen atoms. In the case of an inverse spinel, the A atoms occupy a half of the B sites. This means that for mixed oxide spinels, the site occupation can be represented by $(A_{1-c}B_c)[A_cB_{2-c}]O_4$ where c defines the inversion parameter ($0 \leq c \leq 1$).

For mechanically activated $ZnFe_2O_4$, the key feature is the redistribution of Fe^{3+} into tetrahedral interstices and Zn^{2+} into octahedral interstices. This cationic rearrangement leads to the formation of two (A) and [B] magnetic sublattices which are then responsible for the enhanced magnetisation displayed when compared with normal $ZnFe_2O_4$ in its equilibrium state [e.g. 7]. As explained by several authors, the overall magnetic behaviour can be well accounted for in terms of an exchange interaction of the type $Fe^{3+}(A)$—O^{2-}—$Fe^{3+}[B]$ occurring as a result of this cationic re-distribution in nanoscale $ZnFe_2O_4$ [e.g. 7, 13, 21–23].

Details of the structural features and enhanced magnetisation exhibited by nanoscale $ZnFe_2O_4$ have been extensively investigated by several groups using a variety of techniques including: magnetisation [10, 12, 17–19, 23, 24], Mössbauer spectroscopy [8–12, 16, 18, 21–25], X-ray photoelectron spectroscopy [2], neutron scattering [22, 26–28], muon spin rotation/relaxation [21, 22, 27], extended X-ray absorption fine structure (EXAFS) [13, 29], specific heat [16] and the Faraday effect [19] as well as a range of standard laboratory characterisation techniques. Despite the wealth of insight gleaned from these investigations, a complete understanding of the magnetic behaviour of nanostructured $ZnFe_2O_4$ in its transformation from long range antiferromagnetic order in its equilibrium state (as determined from several investigations [e.g. 21, 30]), to a ferrimagnetic-like behaviour with particle size reduction, has still not been obtained. Indeed, the magnetic properties of equilibrium $ZnFe_2O_4$ itself remain, to some extent, unresolved. Underscoring the enigmatic magnetic behaviour attributed to $ZnFe_2O_4$ by Schiessl *et al.* [21] who considered that $ZnFe_2O_4$ avoided topological frustration by establishing long range antiferromagentic order, Usa *et al.* [31] concluded from recent neutron diffraction studies of $ZnFe_2O_4$ samples of varying quality, that the *absence* of superlattice peaks associated with long range antiferromagnetic order (in particular the pronounced $(10\frac{1}{2})$ peak observed in many neutron studies of equilibrium $ZnFe_2O_4$), characterises the intrinsic behaviour of $ZnFe_2O_4$ [see also 32].

Given the complex interactions occurring in nanostructured $ZnFe_2O_4$, neutron scattering allows good scope for the structural and magnetic changes which take place as the particle size is reduced to be followed. However neutron diffraction investigations have so far only been carried out on a limited number of nanoscale $ZnFe_2O_4$ samples [e.g. 26, 33]. A key feature of our studies of the effects of milling $ZnFe_2O_4$ is investigation of the structural and magnetic changes that take place over a wide range of samples of different particle sizes [25, 28]. Here we report the findings of a neutron diffraction study carried out on a series of 8 nanostructured $ZnFe_2O_4$ samples of mean particle sizes varying from $d \sim 50$ nm to 8 nm over the temperature range 2–535 K. Combined with magnetisation measurements (4.2–300 K), this has led to information on the structural and magnetic changes occurring in mechanically activated $ZnFe_2O_4$. Schematic phase diagrams outlining the main magnetic behaviours of nanostructured $ZnFe_2O_4$ with mean particle size and inversion parameter are presented.

2. Experimental

As outlined previously [25, 28], coarse-grained powders of $ZnFe_2O_4$ (Alfa Aesar) were milled in both a low-energy magnetic mill (LEM; 20, 40, 60, 80 and 120 h) and in a high-energy SPEX 8000 shaker mill (HEM; 2, 4, 6 and 12 h). These combinations of milling energies and times were chosen in order to obtain the required range of particle sizes with a gradual decrease from $d \sim 50$ nm for 20 h LEM to $d \sim 8$ nm for 12 h HEM. Full details about the milling conditions are provided elsewhere [25, 28]. The samples were checked by energy-dispersive X-ray spectroscopy (EDX) and the Fe impurity level found to be <0.1 at.% with no evidence of other impurities. The samples were characterised using Cu K_α radiation and a Siemens Rigaku X-ray diffractometer, leading to mean values of the lattice parameters, inversion parameters and particle sizes [25, 28]. The neutron diffraction measurements were carried out on the E6 diffractometer ($\lambda = 2.441$ Å) at BENSC, Berlin and diffraction patterns were obtained on the ~2–3 g samples over the temperature range 2–535 K using a standard helium cryostat. Several experiments were carried out on MRPD at HIFAR, Lucas Heights. Rietveld refinements of the X-ray and neutron diffraction data were carried out using FULLPROF [34]. Magnetisation measurements were carried out in a field of 0.01 T over the temperature range 4.2–300 K using a Quantum Design SQUID magnetometer in both zero field (ZFC) and field cooling (FC) modes.

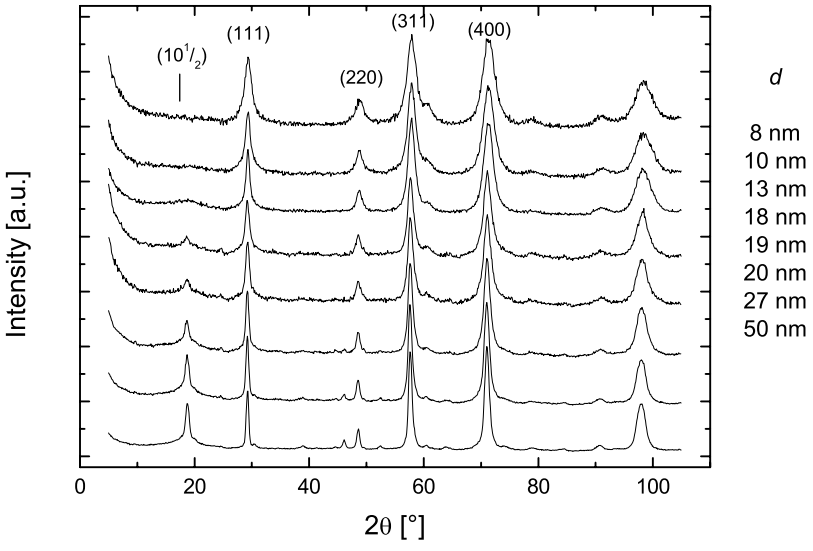

Figure 1 Neutron diffraction patterns of nanostructured $ZnFe_2O_4$ at 2 K. The Miller indices for several nuclear peaks are shown and the mean particle sizes, d, indicated for each sample. The additional magnetic superlattice reflections present in several samples are discussed in the text.

3. Results and discussion

3.1. Nanostructured $ZnFe_2O_4$

Fig. 1 shows the set of neutron diffraction patterns obtained for all of the milled samples at 2 K. As for the corresponding set of room temperature X-ray data [25], the reflections match those of equilibrium $ZnFe_2O_4$ but with increasing line broadening as expected from particle size diminution on milling. Significant differences from the X-ray data are, of course, the additional superlattice reflections in the neutron patterns (e.g. $(10\frac{1}{2})$ associated with the magnetic unit cell as determined by Fayek *et al.* [35] for the antiferromagnetic ordering of $ZnFe_2O_4$; see also the discussion below) and the occurrence of a broad diffuse peak located generally around the $(10\frac{1}{2})$ peak position. Further features are also evident in the 2 K neutron diffraction patterns with decreasing particle sizes—the magnetic intensity of the $(10\frac{1}{2})$ peak decreases, the intensity of the broad diffuse peak decreases, and increased scattering (indicative of a magnetic contribution) is observed in, for example, the (111) reflection.

Given the presence of magnetic scattering in most of the milled samples at 2 K, the initial attempts to refine the neutron diffraction patterns were carried out using the average inversion parameters determined from the X-ray data [25]. This approach should, in principle, allow greater control in refinements for the magnetic contributions to the neutron patterns. In the event unsatisfactory fits to the neutron data were obtained with evident regions of misfit and poor chi-squared values (typically ∼4–5). The neutron data were therefore fitted in the usual way allowing both the cation occupancies and magnetic contributions to be refined. This led to improved quality fits with chi-squared values as low as ∼1.5. Fig. 2 shows examples of the final refinements for the neutron diffraction patterns of the milled samples (Fig. 2a): $d \sim 8$ nm sample at 2 K and 535 K; Fig. 2b: $d \sim 18$ nm sample at 525 K) with the main parameters listed in Table I. As discussed fully below, given the need to heat these samples to ∼530 K to determine the magnetic transition temperatures, the mean particle sizes were also checked from the high temperature refinements. In the case of the $d \sim 8$ nm sample, applying the familiar Scherrer relationship to the (400) reflection leads to $d \sim 9$ nm at ∼535 K; likewise the particle size of the $d \sim 18$ nm sample was found to remain unchanged at ∼525 K (Fig. 2b) compared with the value at room temperature.

The cationic occupancies resulting from the refinements led to mean inversion parameters as listed in Table I which were found to be consistently below (by ∼20–50%) those obtained on refinement of the X-ray data [25]. Using the known values of X-ray and neutron scattering amplitudes, calculated sets of X-ray and neutron diffraction patterns show that, for the same degree of inversion, neutron patterns exhibit significantly larger changes in peak intensities compared with X-ray patterns. As an example, for partially inverted $ZnFe_2O_4$ with an inversion parameter $c = 0.5$, combined changes in intensity of ∼65% are calculated for the 4 main nuclear reflections (111), (220), (222), (400) by neutron diffraction compared with only ∼17% for the same peaks using X-ray diffraction. While X-ray data generally benefit from higher resolution and statistical quality compared with neutron data, the present findings none the less suggest that neutron data provide more reliable inversion parameters for nanostructured $ZnFe_2O_4$ than the corresponding X-ray data; the inversion results and refinements obtained from the neutron data are therefore preferred over those derived from the X-ray data. As is evident in Fig. 1, the patterns exhibit relatively little overlap, thus allowing good peak separation and correspondingly good cationic occupancies in the refinement process. As well, the refinements allow the background scattering to be determined for each pattern with consistency checks showing no change in the refined values (within error) for all samples over the temperature ranges measured.

As discussed by several authors [e.g. 2, 13, 18, 23, 33, 36], values for the inversion parameters of partially inverted $ZnFe_2O_4$ prepared by different methods have been determined by a variety of techniques,

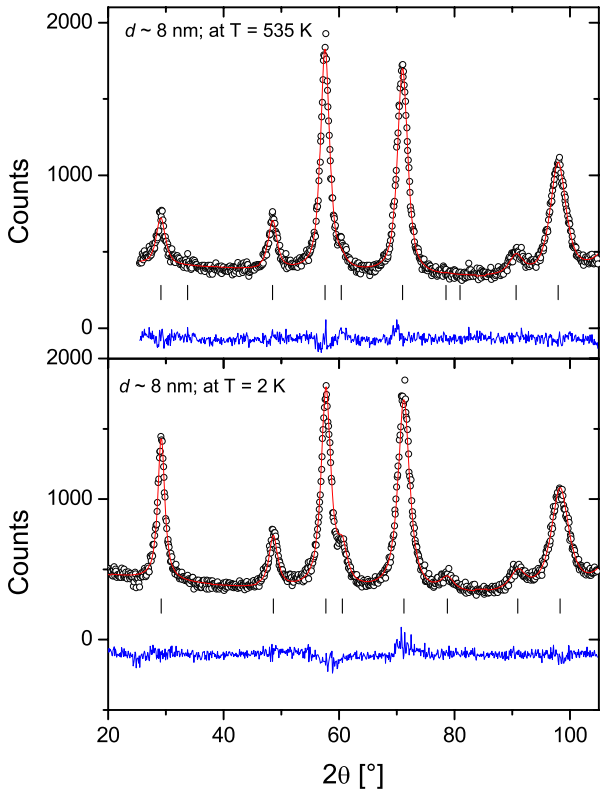

(a)

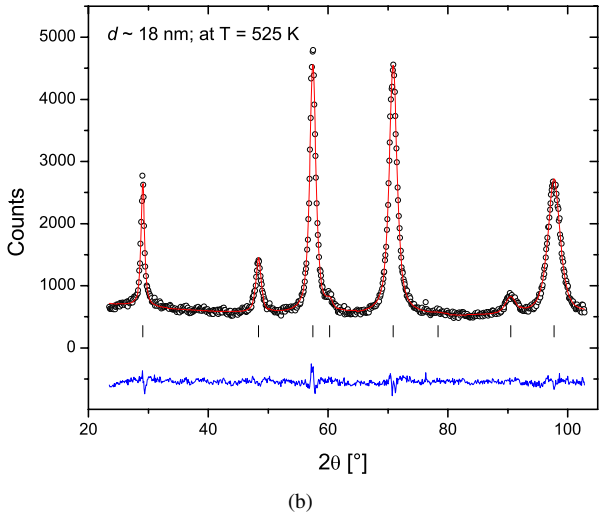

(b)

Figure 2 Examples of the Rietveld refinements to the neutron diffraction patterns of nanostructured $ZnFe_2O_4$ samples: (a) $d \sim 8$ nm at 2 K and 535 K; (b) $d \sim 18$ nm at 525 K.

including X-ray and neutron diffraction, Mössbauer spectroscopy, EXAFS, LEIS and XPS. It should be noted however, that the neutron refinements provide a value for the inversion parameter of the bulk sample as a whole and therefore reflects the atomic distributions on the surfaces of nanograins and in the intergranular regions as well as in the nanograins themselves. Comparison of the inversion parameters determined for the same mechanically treated nanoscale $ZnFe_2O_4$ samples by both X-ray diffraction and the surface sensitive technique of X-ray photoelectron spectroscopy, XPS, shows that $c^{\text{bulk}} > c^{\text{surface}}$ [2]. This difference is due to the high incidence of unsatisfied bonds on the distorted surface structure produced by milling. Given that the intergranular regions in nanostructured materials are also heavily distorted and exhibit distributions of interatomic and hyperfine properties, the present results are considered to represent mean values for the inversion parameters of nanostructured $ZnFe_2O_4$ samples. As outlined below, this has enabled systematic changes in the magnetic behaviour of nanostructured $ZnFe_2O_4$ to be monitored as functions of d and c.

Apart from the magnetic features identified with the antiferromagnetic order of $ZnFe_2O_4$ as discussed briefly above, the main contributions to magnetic scattering are found to occur at the nuclear peak positions of the spinel structure for the milled samples with the smallest particle size. For example, comparison of the patterns for the $d \sim 8$ nm sample at 2 K and 535 K (Fig. 2a) shows increased scattering in the (111) reflection at 2 K consistent with the occurrence of additional magnetic scattering in this sample at low temperatures. Given the increase in inversion parameter with increased mechanical activation and decreasing particle size [e.g. 11, 25] and the commensurate tendency towards an inverse spinel structure, these magnetic features are consistent with ferrimagnetic ordering of the Fe cations on the A and B sites [see e.g. 37].

The neutron diffraction patterns of the 3 samples with the smallest particle sizes are consistent with ferrimagnetic ordering of Fe^{3+} cations in the (A) and [B] sites and Fig. 3a shows the temperature dependence of the magnetic moment associated with the ferrimagnetic model used to refine the $d \sim 8$ nm (12 h HEM) sample. The results indicate a saturated value for the magnetic moment of $\mu = 3.5(1)\ \mu_B$ at 2 K and an ordering temperature of $T_c \sim 490(10)$ K. These findings are similar to those of Schäfer *et al.* [26] who obtained a moment of $\mu = 2.53(6)\ \mu_B$ at 4.2 K and $T_c \sim 460$ K for a nanostructured sample ($d \sim 9$ nm) prepared by mechanical activation. However, in common with these earlier results, the moment determined by neutrons in the present experiments is below that expected on the basis of the magnetic hyperfine splitting observed in Mössbauer measurements [22]. The present

TABLE I Representative values derived from the Rietveld refinements to the nanostructured $ZnFe_2O_4$ samples at the temperatures indicated. The mean particle sizes were determined from the X-ray diffraction data [25]

Milling time (h)	0	20 (LEM)	40 (LEM)	60 (LEM)	120 (LEM)	2 (HEM)	4 (HEM)	12 (HEM)
T (K)	293	150	150	150	525	485	487	535
Inversion, c	0.008(4)	0.04(2)	0.057(20)	0.064(6)	0.097(10)	0.194(19)	0.268(15)	0.431(20)
a-lattice (Å)	8.4126(7)	8.417(1)	8.414(2)	8.406(2)	8.435(1)	8.404(1)	8.400(1)	8.407(4)
u (x,x,x)	0.7359(2)	0.7393(5)	0.7388(7)	0.7383(5)	0.7406(5)	0.7421 (5)	0.7432(5)	0.7430(8)
d [nm] (XRD, see [25])	>100	~50	27(3)	20(2)	18(2)	13(1)	10(1)	8(1)

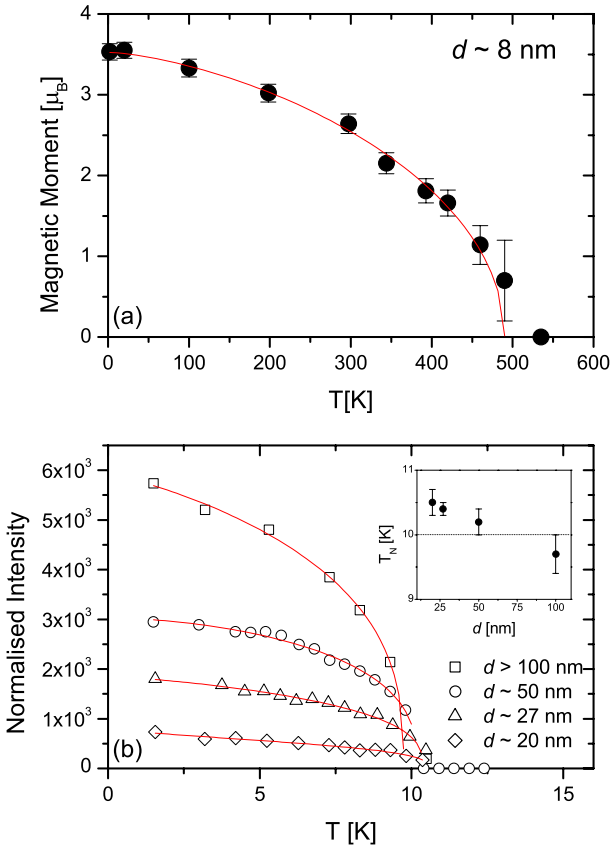

Figure 3 (a) The temperature dependence of the magnetic moment for nanostructured $ZnFe_2O_4$ ($d \sim 8$ nm). (b) Graphs of the variation of the intensity of the $(10\frac{1}{2})$ peak as a function of temperature for the nanostructured $ZnFe_2O_4$ samples indicated (the inset shows T_N as a function of particle size)

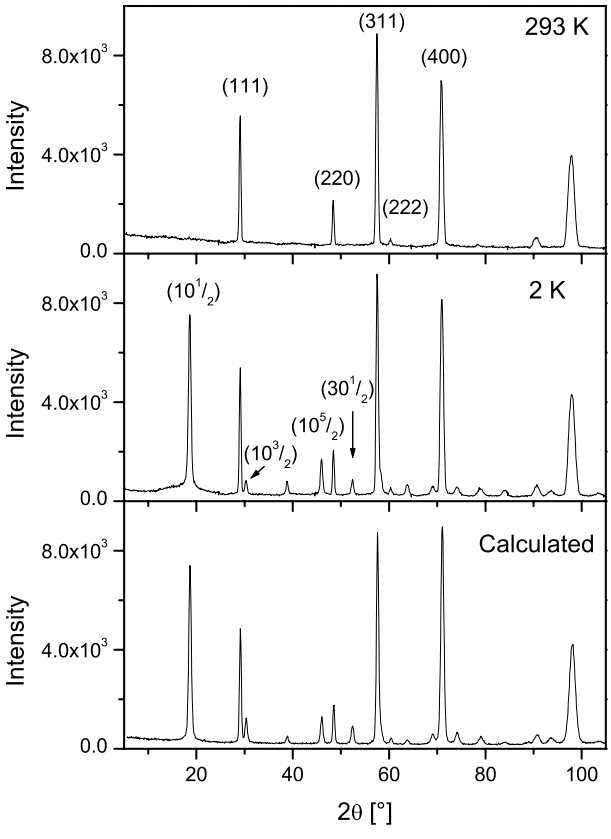

Figure 4 Neutron diffraction patterns of coarse grained $ZnFe_2O_4$ at 293 K (top) and 2 K (middle). Also shown for comparison is the pattern calculated (bottom) on the basis of a tetragonal magnetic structure for $ZnFe_2O_4$ [35].

ferrimagnetic model assumes collinear moments on Fe^{3+} on the (A) and [B] sites and, while representing the diffraction patterns well (e.g. Fig. 2), the model does not accommodate magnetic misalignments due, for example, to spin-canting [16, 33, 38] and surface anisotropy in nanoparticles [39]. While further details are beyond the scope of analyses of the powder diffraction patterns, these results none the less confirm the findings of earlier groups who, on the basis of magnetisation and Mössbauer effect measurements [see e.g. 12, 24 and references therein] concluded that nanoscale $ZnFe_2O_4$ exhibits ferrimagnetic ordering.

3.2. $ZnFe_2O_4$

Despite almost 50 years of investigation [30], the magnetic structure of equilibrium $ZnFe_2O_4$ is still not unequivocally determined (see [21, 40] and references therein for discussion of magnetic models). As shown in Fig. 4, the neutron diffraction pattern which we obtain at 2 K for our commercial sample of coarse grained $ZnFe_2O_4$ is typical of diffraction patterns obtained in several previous investigations [e.g. 12, 31, 35, 41, 42]. The additional magnetic peaks which are associated with a tetragonal magnetic unit cell for $ZnFe_2O_4$ and the propagation vector $[0, 0, \frac{1}{2}]$ are evident on comparison with the room temperature diffraction pattern in Fig. 4. As also shown in Fig. 4, a calculation based on a tetragonal magnetic model [35] describes the observed magnetic superlattice reflections of the present coarse grained $ZnFe_2O_4$ well. However this, or any similar model, is unable to account for the broad peak evident around the $(10\frac{1}{2})$ peak position.

This inability to properly account for these well documented features has been noted by several authors [e.g. 21, 43, 44]. Indeed as noted above, Usa *et al.* [31] have recently concluded that it is the *absence* of long range antiferromagnetic order which characterises the intrinsic behaviour of $ZnFe_2O_4$ and that the magnetic behaviour originates from geometrical frustration and a unique property of the first neighbour interaction [32, 45]. Lee *et al.* [46] have recently presented a detailed analysis of the inelastic neutron scattering from the cubic spinel $ZnCr_2O_4$ in which they report how unusual magnetic composite spin degrees of freedom can emerge from frustrated magnetic interactions in this compound. In particular they demonstrate that the neutrons scatter from hexagonal spin clusters rather than individual spins. Indeed it appears likely that the overall magnetic behaviour of $ZnFe_2O_4$ will ultimately be explained in terms of effects due to geometrical frustration, with spins on the vertices of corner-sharing tetrahedral (i.e. the Fe^{3+} [B] sites) unable to satisfy all interactions [45, 46].

3.3. Magnetic regions of nanostructured $ZnFe_2O_4$

As is evident from Fig. 1, the superlattice peak located at $(10\frac{1}{2})$ and identified with antiferromagnetic ordering in $ZnFe_2O_4$ decreases in intensity with decreasing

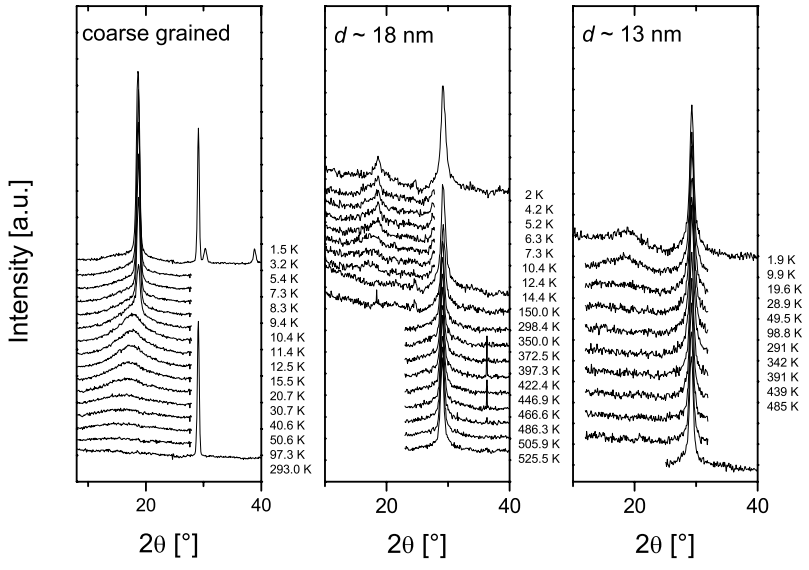

Figure 5 Neutron diffraction scans at the temperatures indicated for: (a) coarse grained $ZnFe_2O_4$; (b) nanostructured $ZnFe_2O_4$ ($d \sim 18$ nm); and (c) nanostructured $ZnFe_2O_4$ ($d \sim 13$ nm).

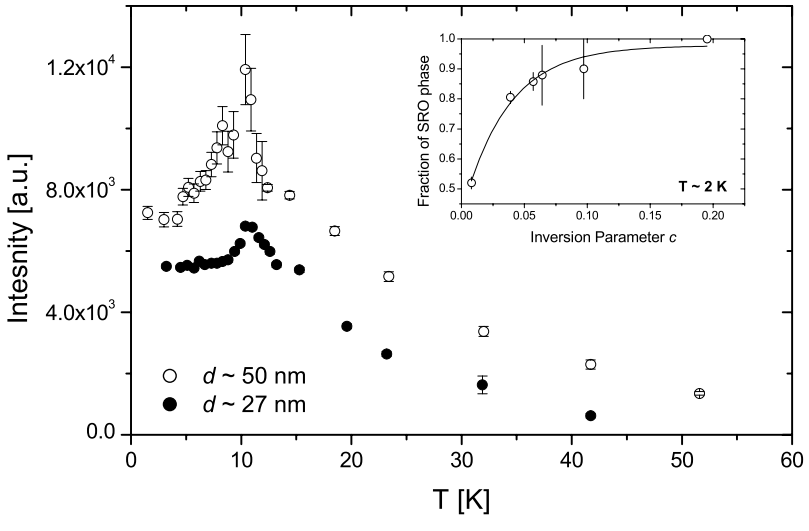

Figure 6 The variation of the intensity of the SRO diffuse peak with temperature for the $d \sim 50$ nm and $d \sim 27$ nm samples. The inset shows the fraction of the SRO diffuse peak (relative to the long range AF order peak) as a function of c.

particle size, as does the diffuse peak located around this peak position. We have investigated the temperature dependence of these features for all samples in order to characterise more fully the magnetic behaviour of nanostructured $ZnFe_2O_4$. Fig. 5 shows examples of the sets of temperature scans obtained for coarse grained $ZnFe_2O_4$ and the $d \sim 18$ nm and $d \sim 13$ nm samples with examples of the temperature dependence of the different magnetic regions of nanostructured $ZnFe_2O_4$ shown in Fig. 6. An AF region is identified with the occurrence of the $(10\frac{1}{2})$ antiferromagnetic reflection, with the diffuse peak identified as short range order (SRO).

As shown in Fig. 4b, T_N, the temperature at which the intensity of the $(10\frac{1}{2})$ peak goes to zero appears to be approximately invariant for all particle sizes with $T_N = 10.0 \pm 0.5$ K. Also the intensity of the SRO diffuse peak is found to have a maximum around T_N (Fig. 6a), demonstrating the close link between the diffuse scattering and the occurrence of the antiferromagnetic $(10\frac{1}{2})$ peak. Fig. 6b shows the fraction of the SRO diffuse peak relative to the long range AF order as a function of inversion parameter. As discussed below, this indicates a continuous change in magnetic character for nanostructured $ZnFe_2O_4$ as the combination of AF order and SRO gives way to ferrimagnetism with increasing cationic inversion.

Summaries of the magnetic features outlined above and the main magnetic regions of nanostructured $ZnFe_2O_4$ produced by mechanical activation are shown in Fig. 7. In coarse grained material the characteristic long range antiferromagnetic order and accompanying SRO diffuse peak give way to a region of decreasing SRO with decrease in particle size (Fig. 7a), with the continuous onset of ferrimagnetic order becoming increasingly evident for particles below $d \sim 15$ nm. This onset of ferrimagnetism corresponds to cationic re-distribution of the Fe^{3+} ions on to the tetrahedral sites and the equivalent re-allocation of Zn^{2+} on to the tetrahedral sites with a degree of inversion of $c \sim 0.2$ (Fig. 7b). Fig. 7b also includes the result obtained for a quenched crystalline $ZnFe_2O_4$ sample of inversion $c = 0.11$ for which no magnetic superlattice reflections were obtained but for which the intensity of the diffuse peak became zero at 25 ± 2 K [26]. This agreement

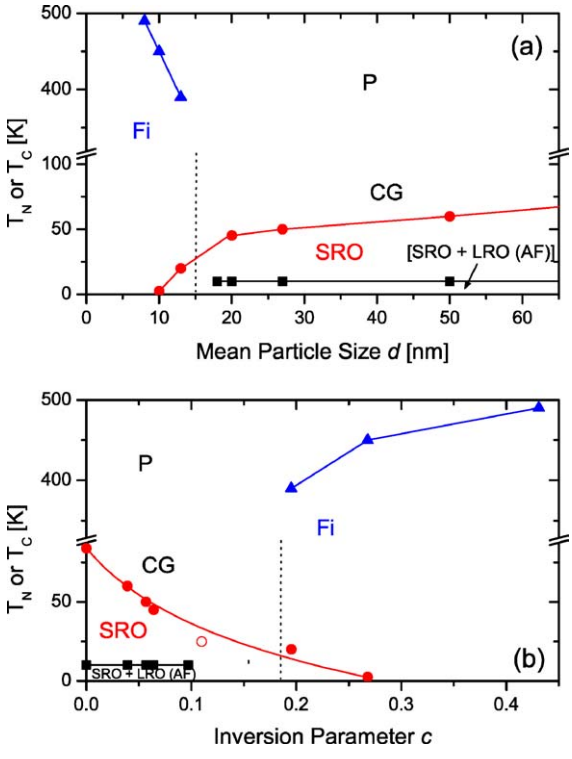

Figure 7 Regions of magnetic behaviour for nanostructured $ZnFe_2O_4$ as functions of: (a) mean particle size d and (b) mean inversion parameter c, as discussed in the text (Fi—ferrimagnetism; CG—cluster glass). The open circle shows the result for a quenched crystalline sample of $ZnFe_2O_4$ [26].

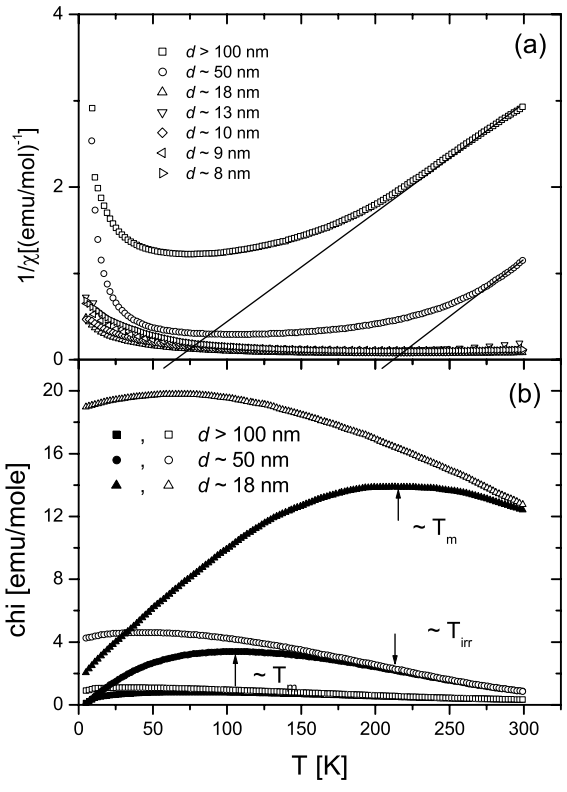

Figure 8 DC magnetic susceptibility and magnetisation data for the nanostructured samples indicated. (a) Inverse susceptibility versus temperature with linear regions indicated for the $ZnFe_2O_4$ and $d \sim 50$ nm samples; (b) Magnetisation versus temperature including both FC (full symbols) and ZFC (open symbols) curves for the samples of particle sizes indicated (T_m and T_{irr} are discussed in the text).

with the results for the partially inverted nanostructured samples demonstrates the validity of this figure in correctly describing the magnetic behaviour of inverted $ZnFe_2O_4$ in both crystalline and nanostructured forms. The overall magnetic behaviour exhibited by nanostructured $ZnFe_2O_4$ is similar to that obtained for substituted Fe^{3+} ferrite systems (see [37] and [47] for experimental and theoretical appraisals respectively), in that the antiferromagnetic order gives way to ferrimagnetism via a spin glass or localised canting state (see e.g. [16] for evidence of a LCS state in partially inverted $ZnFe_2O_4$ fine powders). As indicated by the magnetisation results discussed below, and as also observed in earlier magnetisation studies [e.g. 15, 18, 27], the system otherwise exhibits features similar to those of a cluster glass before reverting to paramagnetism at elevated temperatures.

3.4. Magnetisation of nanostructured $ZnFe_2O_4$

A summary of the magnetisation and magnetic susceptibility data for several nanostructured samples is shown in Fig. 8. As discussed recently [32], equilibrium $ZnFe_2O_4$ characteristically exhibits a peak in susceptibility around 13–20 K [32, 42] while simultaneously showing a positive Curie-Weiss temperature as high as $\theta \sim 120$ K. While discussion of these apparently contradictory effects—antiferromagnetic-like susceptibility compared with positive ferromagnetic-like Curie-Weiss interaction—and the ground state nature of the magnetism of $ZnFe_2O_4$ is continuing [e.g. 22, 32], it is clear that the present $ZnFe_2O_4$ displays similar features with the inverse susceptibility versus temperature graph (Fig. 8a) resulting in the positive value of $\theta \sim 50$ K. While our restricted temperature range from 2 K to a maximum of 300 K prohibits Curie-Weiss analysis of all nanostructured $ZnFe_2O_4$ samples, our magnetisation data demonstrate that milled samples of decreased particle size and increased inversion parameter have an increased θ value compared with $ZnFe_2O_4$ (e.g. $\theta \sim 200$ K for $d \sim 50$ nm, Fig. 8a). This behaviour, combined with the increased values of magnetisation shown with increasing inversion parameter (Fig. 8b), is consistent with the enhanced magnetisation of ferrimagnetism as discussed above.

As demonstrated by the examples in Fig. 8b, all of the nanostructured samples were found to exhibit features consistent with cluster glass-like behaviour. The ZFC magnetisation runs have a broad maximum at T_m in the measuring field of 0.01 T. T_m gives a useful indicator of the blocking temperature, T_B, for each sample although ideally T_B should be measured in low AC magnetic fields (see [48] for discussion of cluster glass behaviour in $Co_{0.2}Zn_{0.8}Fe_2O_4$). All of the nanostructured samples were found to display irreversibility in the FC and ZFC magnetisation curves (see examples in Fig. 8b) although the actual temperature, T_{irr}, at which irreversibility occurs is outside the range of our measurements in several cases. The temperature at which irreversibility sets in tends to increase with increasing inversion as nanostructured $ZnFe_2O_4$ tends increasingly towards ferrimagnetic behaviour.

4. Summary and conclusions

A variable temperature neutron diffraction investigation of a set of partially inverted, nanostructured $ZnFe_2O_4$ samples of mean particle sizes ranging from $d \sim 50$ nm to ~ 8 nm produced by mechanical activation, has enabled the overall magnetic trends of this system to be determined (Fig. 7). The neutron diffraction measurements reveal coexistence of long range antiferromagnetic order and short range order for the larger particles of lower inversion parameter, before the increased inversion of the smaller particles leads to the ferrimagnetism evident in inverted nanostructured samples with $d < \sim 15$ nm. These continuous trends in magnetic behaviour agree well with the enhanced magnetisation and ferrimagnetism reported by several groups for nanoscale $ZnFe_2O_4$ (see Section 1). However the overall magnetic behaviour of nanostructured $ZnFe_2O_4$ is further complicated by the frustration experienced by spins on the vertices of the corner-sharing tetrahedral [B] sites which are unable to satisfy all interactions [46].

A further novel feature observed for nanostructured $ZnFe_2O_4$ is the pronounced forward scattering revealed in the 2 K neutron diffraction patterns (Fig. 1). This scattering changes systematically from sample to sample and appears to exhibit the strongest effect around $d \sim 18$ nm. We are currently undertaking a neutron polarisation analysis of nanostructured $ZnFe_2O_4$; this will allow the nuclear and magnetic diffuse scattering contributions to be separated (particularly the nature of the diffuse peak located around the $(10\frac{1}{2})$ position) and the magnetism of this system to be clarified further. It is clear that investigation of both equilibrium and nanostructured $ZnFe_2O_4$ will continue to interest and challenge experimentalists and theoreticians alike in our attempts to understand fully the structural and magnetic behaviour of this notionally simple, but none the less fascinating system.

Acknowledgements

SJC acknowledges renewal of his Alexander von Humboldt Research Fellowship; his attendance at INCOME2003 was supported in part by the Alexander von Humboldt Foundation. This work was supported in part by a grant from the Australian Institute of Nuclear Science and Engineering. SJC acknowledges several helpful discussions with Dr. W. Potzel.

References

1. V. ŠEPELÁK, K. JANCKE, J. RICHTER-MENDAU, U. STEINIKE, D.-CHR. UECKER and A. YU. ROGACHEV, *Kona* **12** (1994) 87.
2. P. DRUSKA, U. STEINIKE and V. ŠEPELÁK, *J. Solid State Chem.* **146** (1999) 13.
3. M. AHMED, L. ALONSO, J. M. PALACIOS, C. CILLERUELO and J. C. ABANADES, *Solid State Ionics* **138** (2000) 51.
4. S. J. CAMPBELL and W. A. KACZMAREK, in "Mössbauer Spectroscopy Applied to Magnetism and Magnetic Materials," edited by G. J. Long and F. Grandjean (Plenum Press, New York, 1996) Vol. 2, p. 273.
5. YU. T. PAVLJUKHIN, YA. YA. MEDIKOV and V. V. BOLDYREV, *Mater. Res. Bull.* **18** (1983) 1317.
6. K. TKÁCOVÁ, V. ŠEPELÁK, N. ŠTEVULOVÁ and V. V. BOLDYREV, *J Solid State Chem.* **123** (1996) 100.
7. V. ŠEPELÁK, M. ZATROCH, K. TKÁCOVÁ, P. PETROVIC, S. WIßMANN and K. D. BECKER, *Mater Sci. Eng. A* **226–228** (1997) 22.
8. V. ŠEPELÁK, S. WIßMANN and K. D. BECKER, *J. Mater. Sci.* **33** (1998) 2845.
9. *Idem., J. Magn. Magn. Mater.* **203** (1999) 135.
10. G. F. GOYA and H. R. RECHENBERG, *ibid.* 196/197 (1999) 192.
11. J. Z. JIANG, P. WYNN, S. MØRUP, T. OKADA and F. J. BERRY, *Nanostruct. Mater.* **12** (1999) 737.
12. C. N. CHINNASAMY, A. NARAYANASAMY, N. PONPANDIAN, K. CHATTOPADHYAY, H. GUÉRAULT and J.-M. GRENÈCHE, *J. Phys.: Condens. Matter* **12** (2000) 7795.
13. S. A. OLIVER, V. G. HARRIS, H. H. HAMDEH and J. C. HO, *Appl. Phys. Lett.* **76** (2000) 2761.
14. T. SATO, K. HANEDA, M. SEKI and T. IIJIMA, *Appl. Phys. A* **50** (1990) 13.
15. H. H. HAMDEH, J. C. HO, S. A. OLIVER, R. J. WILLEY, G. OLIVERI and G. BUSCA, *J. Appl. Phys.* **81** (1997) 1851.
16. S. A. OLIVER, H. H. HAMDEH and J. C. HO, *Phys. Rev.* B **60** (1999) 3400.
17. S.-H. YU, T. FUJINO and M. YOSHIMURA, *J. Magn. Magn. Mater.* **256** (2003) 420.
18. A. KUNDU, C. UPADHYAY and H. C. VERMA, *Physics Letters* A (in press).
19. K. TANAKA, S. NAKASHIMA, K. FUJITA and K. HIRAO, *J. Phys.: Condens. Matter* **15** (2003) L469.
20. K. E. SICKAFUS, J. W. WILLS and N. W. GRIMES, *J. Amer. Ceram. Soc.* **82** (1999) 3279.
21. W. SCHIESSL, W. POTZEL, H. KARZEL, M. STEINER, G. M. KALVIUS, A. MARTIN, M. K. KRAUSE, I. HALEVY, J. GAL, W. SCHÄFER, G. WILL, M. HILLBERG and R. WÄPPLING, *Phys. Rev.* B **53** (1996) 9143.
22. W. POTZEL, W. SCHÄFER and G. M. KALVIUS, *Hyperfine Interactions* **130** (2000) 241.
23. C. N. CHINNASAMY, A. NARAYANASAMY, N. PONPANDIAN and K. CHATTOPADHYAY, *Mater. Sci. Eng.* A **304–306** (2001) 983.
24. C. N. CHINNASAMY, A. NARAYANASAMY, N. PONPANDIAN, K. CHATTOPADHYAY, H. GUÉRAULT and J.-M. GRENÈCHE, *Scripta Mater.* **44** (2001) 1407.
25. H. EHRHARDT, S. J. CAMPBELL and M. HOFMANN, *J. Alloys Compd.* **339** (2002) 255.
26. W. SCHÄFER, W. KOCKELMANN, A. KIRFEL, W. POTZEL, F. J. BURGHART, G. M. KALVIUS, A. MARTIN, W. A. KACZMAREK and S. J. CAMPBELL, *Mater. Sci. Forum* **321–324** (2000) 802.
27. F. J. BURGHART, W. POTZEL, G. M. KALVIUS, E. SCHREIER, G. GROSSE, D. R. NOAKES, W. SCHÄFER, W. KOCKELMANN, S. J. CAMPBELL, W. A. KACZMAREK, A. MARTIN and M. K. KRAUSE, *Physica* B **289/290** (2000) 286.
28. H. EHRHARDT, S. J. CAMPBELL and M. HOFMANN, *Scripta Materialia* **48** (2003) 1141.
29. B. JEYADEVAN, K. TOHJI and K. NATSUKASA, *J. Appl. Phys.* **76** (1994) 6325.
30. J. M. HASTINGS and M. CORLISS, *Phys. Rev.* **15** (1956) 1008.
31. T. USA, K. KAMAZAWA, S. NAKAMURA, H. SEKIYA, Y. TSUNODA, K. KOHN and M. TANAKA, in "Proc. Eighth Int. Conf. on Ferrites," edited by M. Abe and Y. Yamazaki (Kyoto, 2000) p. 316.
32. K. KAMAZAWA, Y. TSUNODA, H. KADOWAKI and K KOHN, *Phys. Rev.* B **68** 024412 (2003).
33. G. F. GOYA, H. R. RECHENBERG, M. CHEN and W. B. YELON, *J. Appl. Phys.* **87** (2000) 8005.
34. FULLPROF, Program for Rietveld-Refinement of X-ray and Neutron diffraction patterns, by Juan Rodriguez-Carvajal, Laboratoire Leon Brillouin (CEA-CNRS, 2000), http://www-llb.cea.fr/fullweb/fp2k/fp2k.htm.
35. M. K. FAYEK, J. LECIEJEWICZ, A. MURASIK and I. I. YAMZIN, *Phys. Stat. Sol.* **37** (1970) 843.
36. V. ŠEPELÁK, *Ann. Chim. Sci. Mat.* **27** (2002) 61.

37. J. L. DORMANN and M. NOGUES, *J. Phys.: Condens. Matter* **2** (1990) 1223.
38. G. F. GOYA and E. R. LEITE, *ibid.* **15** (2003) 641.
39. Y. LABAYE, O. CRISAN, L. BERGER, J.-M. GRENECHE and J. M. D. COEY, *J. Appl. Phys.* **91** (2002) 8715.
40. C. M. SRIVASTAVA, S. N. SHRINGI and M. VIJAYABABU, *Bull. Mater. Sci.* **6** (1984) 27.
41. U. KÖNIG, E. F. BERTAUT, Y. GROS, M. MITRIKOV and G. CHOL, *Solid State Comm.* **8** (1970) 759.
42. B. BOUCHER, R. BUHL and M. PERRIN, *Phys. Stat. Sol.* **41** (1970) 171.
43. V. G. VOLOGIN, *Sov. Phys. Solid State* **29** (1987) 1339.
44. YU. G. CHUKALKIN and V. R. SHTIRTS, *ibid.* **30** (1988) 1683.
45. Y. YAMADA, K. KAMAZAWA and Y. TSUNODA, *Phys. Rev.* B **66** (2002) 064401.
46. S. H. LEE, C. BROHOLM, W. RATCLIFF, G. GASPAROVIC, Q. HUANG, T. H. KIM and S. W. CHEONG, *Nature* **418** (2002) 856.
47. J. VILLAIN, *Z. Physik* B **33** (1979) 31.
48. V. R. N. BHOWMIK and R. RANGANATHAN, *J. Magn. Magn. Mater.* **248** (2002) 101.

Received 11 September 2003
and accepted 13 January 2004